Geometric Characterization and Experimental Validation of Frictional 3-Contact Equilibrium Stances in Three-Dimensions

Yizhar Or
Dept. of ME, Technion, Israel
izi@tx.technion.ac.il

Elon Rimon
Dept. of ME, Technion, Israel
rimon@tx.technion.ac.il

Abstract— **Quasistatic multi-legged locomotion consists of a sequence of equilibrium postures where the mechanism supports itself against gravity while moving free limbs to new positions. A posture maintains equilibrium if the contacts can passively support the mechanism against gravity. This paper is concerned with computation and graphical characterization of equilibrium postures for mechanisms supported by frictional contacts in a three-dimensional gravitational field. For a given set of contacts, this problem reduces to the computing *feasible region* $\mathcal{R}$, defined as the the center-of-mass positions that maintain equilibrium while satisfying the frictional constraints. This paper continues a previous work by the authors, and provides a new method for computing the boundary of $\mathcal{R}$ for 3-contact stances. The paper also gives physical and geometric interpretations for the boundary of $\mathcal{R}$ and discusses its relation with the classical *support polygon principle*. Finally, the paper reports experimental results that validate the theoretical computation.**

I. INTRODUCTION

Multi-legged robots that perform quasistatic locomotion are becoming progressively more sophisticated. This type of locomotion can be characterized as a sequence of postures where the mechanism supports itself against gravity while moving free limbs to new foothold positions. Autonomous planning of these motions requires tools for selecting postures that can stably support the mechanism against gravity while allowing motion of its free limbs to new positions. This paper focuses on computation and graphical characterization of equilibrium postures of multi-legged mechanisms supported by three frictional contacts in a three-dimensional gravitational field. As a first step, the kinematic structure of the mechanism is lumped into a single rigid body $\mathcal{B}$ having the same contacts with the environment and a variable center-of-mass. The identification of the feasible equilibrium postures associated with a given set of contacts is then reduced to the identification of center-of-mass locations that generate feasible equilibrium stances of $\mathcal{B}$, while satisfying friction constraints at the contacts.

Stance stability received considerable attention in the literature discussing multi-legged locomotion. Notable early papers on multi-legged machines are [7], [13]. More recent papers that discuss stance stability appear in the literature on humanoid robots, e.g. [5], [12]. When considering stance stability of legged robots, a classical concept is the *support polygon principle* [7], which states that the center-of mass must lie above the polygon spanned by the contacts. This principle was further extended for dynamic motion synthesis of humanoid robots with the concept of *zero moment point* (ZMP)

[13]. However, these notions apply only for *flat* terrains, where contact normals are purely vertical. Mason et. al. [6] computed equilibrium postures on non-flat terrains in 3D, assuming frictionless contacts. For the frictional case, Or and Rimon [10] characterized robust equilibrium postures in 2D. Only recently, Or and Rimon [8] provided exact computation of frictional equilibrium stances on non-flat terrain in 3D, and Bretl and Lall [2] presented an efficient algorithm for adaptive approximation of such stances.

In the grasping literature, discussing frictional grasps in 3D, some works use polyhedral approximation of the quadratic friction cones [4],[11]. This approach enables formulation of equilibrium and grasp optimization as linear programs. Han et. al. [3] formulated the exact frictional constraints as a linear matrix inequality (LMI) problem, for testing force-closure and optimizing actuator torques. Using a different approach, Bicchi [1] formulated the force-closure test as a nonlinear differential equation. However, these works assume that the geometry of the grasped object is entirely known, while multi-legged mechanisms have a variable shape, which, in this paper, is modelled as a variable center-of-mass, whose position affects the static contact forces.

This paper is a continuation of work reported in [8], which gives an exact algebraic formulation for the boundary of the center-of-mass feasible region, denoted $\mathcal{R}$. This earlier work lacks a physical and geometric interpretation of the boundary. The main contributions of this paper are as follows. First, it provides a new method for computing the boundary of $\mathcal{R}$ for 3-contact stances. Second, it gives physical and geometric interpretations for the boundary of $\mathcal{R}$. Third, it reports experimental results for a 3-legged prototype supported by a frictional terrain, that validate the theoretical computation.

The structure of the paper is as follows. The next section defines the feasible center-of-mass region $\mathcal{R}$ and reviews some of its fundamental properties. Section III reviews the *support polygon principle* and discusses its relation with the feasible region $\mathcal{R}$ for 3-legged stances. Section IV describes a new method for computing the boundary of $\mathcal{R}$, and provides physical and geometric interpretations for this boundary. Section V presents experimental results. Finally, the closing section discusses some future extensions of the work.

II. DEFINITION OF EQUILIBRIUM STANCES IN 3D

This section defines basic terminology and formulates the stance equilibrium condition in 3D. Then it defines the fea-

sible region of center-of-mass locations achieving equilibrium stances, and reviews some of its basic properties. Let a 3D object $\mathcal{B}$ be supported by k frictional contacts under gravity. Let x_i be the position of the ith contact, and let f_i be the ith contact reaction force. The stance equilibrium condition is given by

$$\sum_{i=1}^{k} \left(\begin{array}{c} I \\ [x_i \times] \end{array} \right) f_i = - \left(\begin{array}{c} I \\ [\boldsymbol{x} \times] \end{array} \right) f_g \qquad (1)$$

where $\boldsymbol{x}$ is the position of $\mathcal{B}$'s center-of-mass, f_g is the gravitational force acting at $\boldsymbol{x}$, I is the 3×3 identity matrix, and $[a \times]$ is the cross-matrix satisfying $[a \times]v = a \times v$ for all $v \in I\!\!R^3$. Assuming Coulomb's friction model, the contact forces f_i must lie in their respective friction cones $\mathcal{C}_i$, defined as

$$\mathcal{C}_i = \{f_i : f_i \cdot n_i \geq 0 \text{ and } (f_i \cdot s_i)^2 + (f_i \cdot t_i)^2 \leq (\mu f_i \cdot n_i)^2\}, \ (2)$$

where μ is the coefficient of friction, n_i is the outward unit normal at x_i, and s_i, t_i are unit tangents at x_i such that (s_i, t_i, n_i) is a right-handed frame. We assume μ is a known constant. A 3D stance is defined by the contact points $x_1 \ldots x_k$ and the center-of-mass position $\boldsymbol{x}$. For a given set of contacts, the 3D feasible equilibrium region, denoted $\mathcal{R}$, is all center-of-mass locations for which there exist contact reaction forces $f_i \in \mathcal{C}_i$ satisfying the static equilibrium condition (1). First, we review some fundamental properties of $\mathcal{R}$, summarized in the following proposition.

Proposition II.1 ([8]). *Let a 3D object $\mathcal{B}$ be supported by k frictional contacts against gravity. If the feasible equilibrium region $\mathcal{R}$ is nonempty, it is an infinite vertical prism. This prism is a single connected set and its cross-section is convex. Furthermore, its dimension for k contacts is generically $\min\{3, k\}$.*

It is worth noting that for a single contact $\mathcal{R}$ is a vertical line through the contact, and for two contacts it is a vertical strip in the plane passing through the contacts. For $k \geq 3$ contacts $\mathcal{R}$ is a vertical prism whose position has no obvious relation to the position of the contacts. However, in the special case where all friction cones contain the upward vertical direction, the prism $\mathcal{R}$ contains the contacts. This special case is related to the familiar support polygon principle discussed in the next section.

The problem of computing the prism $\mathcal{R}$ is thus reduced to computing its horizontal cross-section, denoted $\widetilde{\mathcal{R}}$, in $I\!\!R^2$. Since $k = 3$ is the smallest number of contacts for which $\mathcal{R}$ is fully three-dimensional, this paper focuses on the computation of $\widetilde{\mathcal{R}}$ for 3-contact stances, while the concluding section discusses extension of the computation to multiple contacts.

III. RELATION TO SUPPORT POLYGON PRINCIPLE

The support polygon principle appears in the early quasi-static locomotion literature as a posture stability criterion over flat horizontal terrains [7]. It states that $\mathcal{B}$'s center-of-mass must lie in a vertical prism, denoted Π, which is spanned by the contacts. The support polygon, denoted $\widetilde{\Pi}$, is defined as the horizontal projection of Π. In the following, we show that *on non-flat frictional terrains, the support polygon principle may yield non-equilibrium stances.* We revisit the support polygon principle for 3-legged stances on general frictional terrains, and characterize the stances for which $\mathcal{R} \subseteq \Pi$ and/or $\Pi \subseteq \mathcal{R}$.

We will use the following definitions. First, $\boldsymbol{e} = (0\ 0\ 1)$ denotes the upward vertical direction. A contact x_i is defined as *quasi-flat* if $\boldsymbol{e} \in \mathcal{C}_i$. A stance is defined as *quasi-flat* if all its contacts are quasi-flat (Fig 1(a)). Second, the *base plane* $\mathcal{B}_o$ denotes the plane passing through the three contact points in $I\!\!R^3$, and n_o denotes the normal to $\mathcal{B}_o$, chosen such that $\boldsymbol{e} \cdot n_o \geq 0$. A 3-legged stance is defined as *tame* if $\boldsymbol{e} \cdot n_o > 0$ and all forces $f_i \in \mathcal{C}_i$ satisfy $f_i \cdot n_o > 0$ for $i = 1, 2, 3$. The following theorem determines the relation between $\mathcal{R}$ and Π.

Theorem 1 ([9]). *Let a 3D object $\mathcal{B}$ be supported by three frictional contacts in equilibrium against gravity. Let $\mathcal{R}$ be the feasible equilibrium region, and let Π be the vertical prism spanned by the contacts. Then:*
1) *For quasi-flat stances, $\Pi \subseteq \mathcal{R}$*
2) *For tame stances, $\Pi \supseteq \mathcal{R}$.*

This paper focuses on tame stances, for which $\mathcal{R} \subseteq \Pi$ When the terrain is nearly horizontal and the coefficient of friction μ is sufficiently large, all contacts are quasi-flat. In this case Theorem 1 implies that $\mathcal{R} = \Pi$, and the classical support polygon principle holds true. However, when the contact normals are more inclined or when μ is smaller, the support polygon is larger than the feasible region $\mathcal{R}$, as shown in the following examples.

Graphical examples: Fig. 1(a) shows a 3-contact tame stance with coefficient of friction $\mu = 0.7$. In this case, all contacts are quasi-flat, hence the feasible region $\mathcal{R}$ is precisely the prism Π. However, decreasing of μ significantly changes the properties of $\mathcal{R}$ and its horizontal cross-section $\widetilde{\mathcal{R}}$. Fig. 1(b) shows a top view of the same 3-contact stance, with $\mu = 0.5$. Let $\tilde{x}_i$ and $\tilde{\mathcal{C}}_i$ denote the horizontal projections of the contacts x_i and the friction cones $\mathcal{C}_i$ (for convenience, the symbol '$\sim$' is omitted in the labelling inside the figures). Note that in this case the contacts x_1 and x_2 are quasi-flat, while x_3 is not. Therefore, the horizontal projections $\tilde{\mathcal{C}}_1$ and $\tilde{\mathcal{C}}_2$ span the entire plane, while $\tilde{\mathcal{C}}_3$ is a planar sector. Since $x_1, x_2 \in \mathcal{R}$, the whole line segment $\tilde{x}_1 - \tilde{x}_2$ lies on the boundary of $\widetilde{\mathcal{R}}$. However, $x_3 \notin \mathcal{R}$, hence only parts of the segments $\tilde{x}_1 - \tilde{x}_3$ and $\tilde{x}_2 - \tilde{x}_3$ lie on the boundary of $\widetilde{\mathcal{R}}$, ending at the points $\tilde{p}_1$ and $\tilde{p}_2$. The line segment $\tilde{x}_i - \tilde{p}_i$ for $i = 1, 2$ is a horizontal projection of a planar vertical strip, which is precisely the feasible equilibrium region associated with two active contacts at x_i and x_3. This vertical strip can be computed by applying the planar methods shown in [10] while the contact forces are restricted to lie within the vertical plane passing through x_i and x_3. Note that *there is an unknown missing part in the boundary of $\widetilde{\mathcal{R}}$, between $\tilde{p}_1$ and $\tilde{p}_2$.* Fig. 1(c) shows the horizontal projection of contact normals and friction cones for $\mu = 0.4$. Since the projected cone $\tilde{\mathcal{C}}_3$ does not contain $\tilde{x}_2$, contacts x_2 and x_3 alone cannot balance any gravitational load,
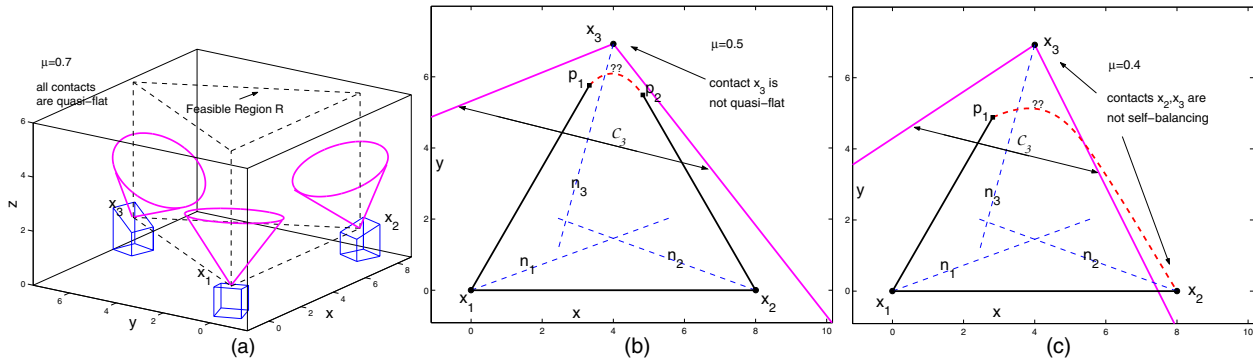
Fig. 1.   (a) A 3-legged tame stance for $\mu = 0.7$, and its horizontal projections for (b) $\mu = 0.5$ and (c) $\mu = 0.4$.

and the segment $\tilde{x}_2 - \tilde{x}_3$ lies outside $\widetilde{\mathcal{R}}$. As before, contacts x_1 and x_3 contribute the segment $\tilde{x}_1 - \tilde{p}_1$, and there is an unknown missing part between $\tilde{p}_1$ and $\tilde{x}_2$.

In these examples the support polygon principle is obviously an *over-approximation* of the feasible region $\mathcal{R}$. Therefore, it is unsafe to apply this principle for non-flat terrains with low friction. The objective of the next section is to compute the exact feasible region $\mathcal{R}$ on non-flat frictional terrain. In particular, it computes the boundaries of the horizontal cross-section $\widetilde{\mathcal{R}}$ associated with three contacts, and provides its physical and geometric interpretations. geometric interpretation.

IV. COMPUTING THE FEASIBLE EQUILIBRIUM REGION

This section presents a new method for computing the feasible equilibrium region. In this method $\widetilde{\mathcal{R}}$ is formulated as an intersection of a six-dimensional cone and an affine two-dimensional subspace in wrench space. Let *wrench space* have force-and-torque coordinates $(f, \tau) \in I\!\!R^6$. As $\mathcal{B}$'s center-of-mass varies in physical space, the gravitational wrench on the right side of (1) spans a two-dimensional affine subspace in wrench space (the component of x along e is mapped to zero). Let L denote this subspace. On the other hand, as the contact forces vary in their friction cones, their net reaction wrench on the left side of (1) spans a cone in wrench space. Let N denote this cone. The intersection $N \cap L$ is generically a two-dimensional region in wrench space. This region contains all net wrenches that can be generated by the contact forces, and balance the wrench of gravitational force acting at x. Any wrench $(f, \tau) \in N \cap L$ is associated with a single center-of-mass horizontal position $\tilde{x}$, via the linear mapping $\tau = -x \times f_g$. Therefore, the horizontal cross section $\widetilde{\mathcal{R}}$ is fully determined by the region $N \cap L$ in wrench space. Since $N \cap L$ is convex, the problem reduces to computation of its one-dimensional boundary. This computation is conducted in three stages, as follows. First we characterize the *equilibrium contact forces*, which are contact forces generating wrenches that lie on the affine subspace L. Then we characterize *critical contact forces*, which are contact forces generating wrenches that lie on the five-dimensional boundary of the wrench cone N. Finally we compute the *critical equilibrium contact forces*, generating wrenches that lie on the boundary of $N \cap L$, and formulate the boundary curves of $\widetilde{\mathcal{R}}$. The results

are demonstrated graphically for the 3-contact arrangement depicted in Fig. 1.

A. Characterizing Equilibrium Contact Forces

We now characterize the contact forces generating wrenches that lie on the affine subspace L. Such contact forces balance the gravitational force f_g, and generate zero torque about the vertical axis. The characterization of such contact forces is given in the following lemma.

Lemma IV.1. *[[9]] Given a 3-legged tame stance with contacts at x_1, x_2, x_3, the contact forces f_1, f_2, f_3 generate a wrench that lies on L if and only if they satisfy the following conditions:*
1. *A single nonzero contact force f_i generates a wrench that lies on L if and only if $f_i = -f_g$.*
2. *Two nonzero contact forces f_i and f_j generate a wrench that lies on L if and only if they lie in the vertical plane that passes through the contacts x_i and x_j, and satisfy $f_i + f_j = -f_g$.*
3. *Three nonzero contact forces f_i and f_j generate a wrench that lies on L if and only if they satisfy*

$$f_1 + f_2 + f_3 = -f_g, \text{ and } \det[H_1 f_1 \ H_2 f_2 \ H_3 f_3] = 0, \text{ where}$$

$$H_i = \begin{pmatrix} E^T \\ e^T[x_i \times] \end{pmatrix} \text{ for } i = 1, 2, 3, \text{ and } E = \begin{pmatrix} 1 & 0 \\ 0 & 1 \\ 0 & 0 \end{pmatrix}. \tag{3}$$

Note that three nonzero contact forces that balance f_g and generate zero torque about the vertical axis, are characterized by the fact that they all intersect a common vertical line. This condition is formulated in the second part of (3).

B. Characterizing Critical Contact Forces

We now characterize the contact forces generating wrenches that lie on the boundary of the cone N. The cone N consists of all wrenches generated by contact forces that satisfy the frictional constraints, and can be formulated as

$$N = \{w = \sum_{i=1}^{3} \begin{pmatrix} f_i \\ x_i \times f_i \end{pmatrix}, \ f_i \in \mathcal{C}_i\}. \tag{4}$$

This cone is generically six-dimensional, and our goal is to compute the contact forces f_i generating wrenches that lie on its five-dimensional boundary. As a preliminary step, let us

define some additional notations. Recall that the base plane $\mathcal{B}_o$ was defined as the plane passing through the contacts, and that n_o denotes the normal to $\mathcal{B}_o$. Let s_o and t_o denote two orthogonal unit vectors in $\mathcal{B}_o$, such that (s_o, t_o, n_o) is a right-handed frame. Finally, let $E_o = I - n_o n_o^T$ denote the matrix that projects vectors in $I\!R^3$ onto $\mathcal{B}_o$, and define $R_{90} = I + [n_o \times] + [n_o \times]^2$ as the 90°-rotation matrix about n_o. Each nonzero contact force f_i that lies on the boundary of its friction cone can be parametrized by the pair $(c_i, \phi_i) \in I\!R^+ \times [0, 2\pi)$ as

$$f_i = c_i u_i(\phi_i), \text{ where } u_i(\phi_i) = \mu \cos(\phi_i) s_i + \mu \sin(\phi_i) t_i + n_i. \tag{5}$$

Let $\mathcal{B}_i(\phi_i)$ denote the plane tangent to the boundary of $\mathcal{C}_i$ that contains $u_i(\phi_i)$, and let l_{i0} denote the line of intersection between the planes $\mathcal{B}_i(\phi_i)$ and $\mathcal{B}_o$. Finally, define $M_i = I - (1 + \mu^2) n_i n_i^T$. It can then be verified that $M_i u_i(\phi_i)$ is normal to $\mathcal{B}_i(\phi_i)$, and that the vector defined by $l_i(\phi_i) = R_{90} E_o M_i u_i(\phi_i)$ is parallel to l_{i0}.

The following lemma formulates three different types of critical contact forces associated with five-dimensional boundary cells of N, and provides their geometric interpretation.

Lemma IV.2 ([9]). *Given a 3-legged tame stance with contacts at x_1, x_2, x_3 and their friction cones $\mathcal{C}_1, \mathcal{C}_2, \mathcal{C}_3$, there are three types of critical contact forces. The critical forces are associated with three different types of five-dimensional boundary cells of the wrench cone N, and are formulated as follows:*
1. *Type-1 critical contact forces consist of one zero force and two nonzero forces varying freely within their friction cones.*
2. *Type-2 critical contact forces consist of one nonzero force f_1 varying freely within its friction cone $\mathcal{C}_1$, and two nonzero forces lying on the boundaries of their friction cones. The two forces f_2 and f_3 have fixed directions, and are parametrized by $f_2 = c_2 u_2(\phi_2^*)$, $f_3 = c_3 u_3(\phi_3^*)$ (the contacts' indices may be arbitrarily permuted). The fixed directions $u_2(\phi_2^*)$ and $u_3(\phi_3^*)$ are determined such that the lines l_{20} and l_{30} pass through the contact point x_1. This condition is formulated as follows:*

$$n_o \cdot (x_i - x_1) \times l_i(\phi_i^*) = 0 \;\;, i = 2, 3,$$
$$\text{where } l_i(\phi_i) = R_{90} E_o M_i u_i(\phi_i) \tag{6}$$

3. *Type-3 critical contact forces are three nonzero forces lying on the boundaries of their friction cones, and parametrized by $f_i = c_i u_i(\phi_i), i = 1, 2, 3$. The forces are directed such that the three lines l_{i0} all intersect at a common point. This condition is formulated as follows:*

$$\det[E_1 l_1(\phi_1) \; E_2 l_2(\phi_2) \; E_3 l_3(\phi_3)] = 0,$$
$$\text{where } E_i = \begin{pmatrix} s_o^T \\ t_o^T \\ n_o^T [x_i \times] \end{pmatrix} \;\;, i = 1, 2, 3. \tag{7}$$

C. Computing the Boundary Curves of $\widetilde{\mathcal{R}}$

We now complete the computation of the boundary curves of $\widetilde{\mathcal{R}}$. The *equilibrium forces* generating wrenches that lie on the affine subspace L are formulated in Lemma IV.1. The *critical forces* generating wrenches that lie on the boundary of

the wrench cone N are formulated in Lemma IV.2. Combining these two conditions together gives rise to *critical equilibrium forces*, generating wrenches that lie on candidate boundary curves of the intersection $N \cap L$. Recall that $\tilde{x} = E^T x$ denotes the center-of-mass horizontal projection. Using the equilibrium condition (1), the candidate boundary curves of $\widetilde{\mathcal{R}}$ can be obtained from the critical equilibrium forces f_1, f_2, f_3 via the linear mapping

$$\tilde{x} = J^T E^T \sum_{i=1}^{3} x_i \times f_i, \text{ where } J = \begin{bmatrix} 0 & -1 \\ 1 & 0 \end{bmatrix}.$$

The formulation of candidate boundary curves of $\widetilde{\mathcal{R}}$ is summarized in the following corollary.

Corollary IV.3. *Let a 3D object $\mathcal{B}$ be supported by three frictional contacts in equilibrium against gravity in a tame stance. Then the feasible equilibrium region $\mathcal{R}$ is a vertical prism with a horizontal cross-section $\widetilde{\mathcal{R}}$, whose candidate boundary curves are of the three types listed below.*
1. *Type-1 boundary curves occur when the horizontal projection of two friction cones $\tilde{\mathcal{C}}_i$ and $\tilde{\mathcal{C}}_j$ contain the projected contacts $\tilde{x}_i$ and $\tilde{x}_j$. In such cases, type-1 boundary curve is a line segment lying on the edge $\tilde{x}_i - \tilde{x}_j$, whose endpoints can be computed by using the planar methods described in [10].*
2. *Type-2 candidate boundary curves are straight line segments parametrized by $s \in [0, 1]$ as*

$\tilde{x} = J^T E^T \sum_{i=1}^3 x_i \times f_i(s)$, *where s*
is additionally restricted such that $f_i(s) \in \mathcal{C}_i$ for $i = 1, 2, 3$,
where $f_1(s) = s c_1^a u_1(\phi_1^a) + (1 - s) c_1^b u_1(\phi_1^b)$,
$f_i(s) = (s c_i^a + (1 - s) c_i^b) u_i(\phi_i^*)$, *for $i = 2, 3$,*
c_i^a *and c_i^b are solutions of the linear systems*
$c_1^a u_1(\phi_1^a) + c_2^a u_2(\phi_2^*) + c_3^a u_3(\phi_3^*) = -f_g$
$c_1^b u_1(\phi_1^b) + c_2^b u_2(\phi_2^*) + c_3^b u_3(\phi_3^*) = -f_g$,
ϕ_2^* *and ϕ_3^* are solutions of (6),*
and ϕ_1^a, ϕ_1^b are the two solutions for ϕ_1 in the equation
$\det \begin{bmatrix} H_1 u_1(\phi_1) & H_2 u_2(\phi_2^*) & H_3 u_3(\phi_3^*) \end{bmatrix} = 0$,
where H_i are defined in (3), $u_i(\phi_i)$ are defined in (5),
and the contacts' indices can be arbitrarily permuted.

3. *Type-3 candidate boundary curves are formulated as*

$\tilde{x} = J^T E^T \sum_{i=1}^3 c_i x_i \times u_i(\phi_i)$, *where c_i are solutions of*
$c_1 u_1(\phi_1) + c_2 u_2(\phi_2) + c_3 u_3(\phi_3) = -f_g$,
and ϕ_1, ϕ_2, ϕ_3 are the solution set of the equations
$\det \begin{bmatrix} H_1 u_1(\phi_1) & H_2 u_2(\phi_2) & H_3 u_3(\phi_3) \end{bmatrix} = 0$, *and*
$\det \begin{bmatrix} E_1 l_1(\phi_1) & E_2 l_2(\phi_2) & E_3 l_3(\phi_3) \end{bmatrix} = 0$, *such that $c_i > 0$,*
where H_i are defined in (3), $u_i(\phi_i)$ are defined in (5),
and $E_i, l_i(\phi_i)$ are defined in (7).

We now provide physical meaning for each type of boundary curves. When the center-of-mass x is located on the boundary of $\mathcal{R}$, the reaction forces that generate equilibrium are also
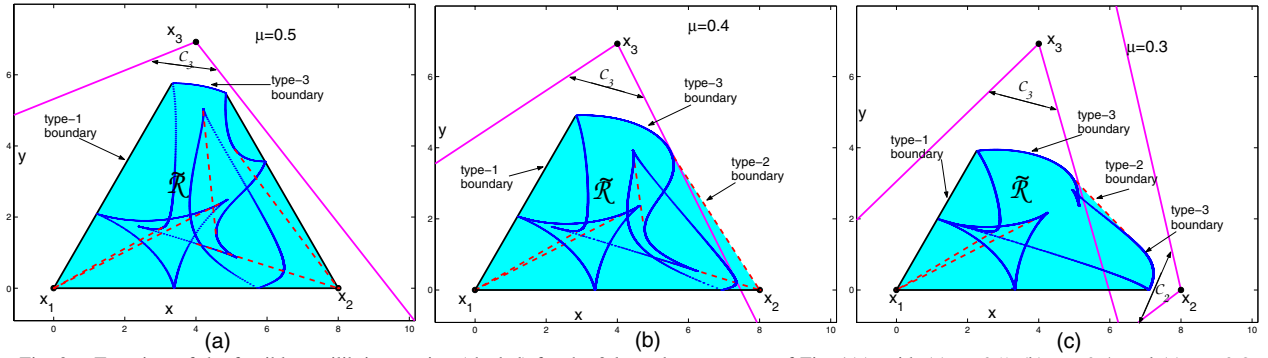
Fig. 2. Top view of the feasible equilibrium region (shaded) for the 3-legged tame stance of Fig. 1(a), with (a)$\mu = 0.5$, (b) $\mu = 0.4$, and (c) $\mu = 0.3$.

consistent with the onset of a non-static motion. Each type of boundary curve corresponds a different imminent motion, as follows. Type-1 boundary curves are associated with two nonzero contact forces lying within their friction cones and a zero force at the third contact. These curves correspond to tipping-over motion of the mechanism, involving pure rolling about two contacts and breakage of the third contact. Type-2 boundary curves are associated with two contact forces lying on the boundaries of their friction cones, while the third contact force lies within its friction cone. These curves correspond to onset of sliding on two contacts and pure rolling about the third contact. Type-3 boundary curves are associated with three nonzero contact forces lying on boundary of their friction cones. These curves correspond to onset of simultaneous sliding at all three contacts.

Graphical examples: Fig. 2(a),(b),(c) show the horizontal cross section $\widetilde{\mathcal{R}}$ (shaded region) for $\mu = 0.5, 0.4, 0.3$ respectively, with the contact arrangement of Fig. 1(a). The boundary of $\widetilde{\mathcal{R}}$ consists of type-1 line segments (thick lines), type-2 line segments (dashed lines), and type-3 curves (solid). Note that type-1 and type-2 boundary curves are easy to compute in closed-form. However, for computing type-3 boundary curves, one needs to find the one-dimensional solution set of two nonlinear equations in (ϕ_1, ϕ_2, ϕ_3), which does not have a closed-form formulation. In [9] we present a scheme for numerical computation of these boundary curves by defining the variables $\beta_i = \tan(\phi_i/2)$ and using standard elimination methods on the two equations in (7) to obtain a single polynomial of degree 16 in (β_1, β_2), which is solved numerically.

V. EXPERIMENTAL RESULTS

This section describes preliminary experiments that measure the feasible equilibrium region of a three-legged prototype supported by a frictional terrain. The experimental system, shown in Fig. 3(a), consists of a three-legged mechanism made of Aluminium. The mechanism consists of an annular frame and three extendable legs with spherical footpads, making point contacts with three Aluminium plates. A heavy steel cylinder moves along a horizontal linear slider, which is mounted on top of the annular frame. The three supporting plates maintain fixed position and adjustable slopes, such that the contact normals can be varied. The dimensions of the mechanisms are as follows. The diameter of the annular frame

is 212 mm. The nominal length of the legs is 180 mm, and the length of the linear slider is 430 mm. The total weight of the mechanism is 7.9 Kg, while the movable cylinder weighs 4.2 Kg.

After placing the mechanism on the supporting plates, the heavy cylinder is moved continuously along the slider, thus varying the center-of-mass along a straight line. The center-of-mass is moved until reaching the boundary of the feasible equilibrium region, where a critical event of contact breakage or slippage is observed. The critical center-of-mass position is then recorded, and the process is repeated with the linear slider mounted in different angles on the annular frame. The slider's angles eventually span the whole 360° range with resolution of 15°. This enables mapping of discrete points on the boundary of $\widetilde{\mathcal{R}}$, and comparing these points with the theoretical results for a given contact arrangement.

The contact points are positioned at equal heights, making an equilateral triangle in a horizontal plane, with edge length of 165 mm. The supporting plates at x_1 and x_2 are horizontal, such that n_1 and n_2 are purely vertical. The support at x_3 is rotated such that n_3 makes a 30° angle with the vertical upward direction, and its horizontal projection makes a 20° angle with the bisector of the equilateral triangle in a horizontal plane. As a preliminary step, the coefficient of friction was determined to be $\bar{\mu} = 0.26$ with a standard deviation of $\sigma = \pm 13.2\%$. Fig. 3(b) shows a top view of the contacts and the horizontal projection of the friction cone $\mathcal{C}_3$ for the given contact arrangement (since x_1 and x_2 are flat, the horizontal projection of $\mathcal{C}_1$ and $\mathcal{C}_2$ span the entire plane). The theoretical region $\widetilde{\mathcal{R}}$, computed for with $\mu = \bar{\mu}$, appears as a shaded region. Note that the boundary of $\widetilde{\mathcal{R}}$ consists of curves of all three types. Hence one expects three qualitatively distinct critical events in the experiment. In the experiment, the boundary of $\widetilde{\mathcal{R}}$ is mapped by discrete points that lie along rays emanating from the geometric center of the equilateral triangle formed by the contacts. For each angle of the linear slider, ten measurements were recorded. Fig. 3(c) shows the experimentally measured center-of-mass critical positions, together with the theoretical results. The experimental measurements are marked by '×', while the theoretical boundaries of $\widetilde{\mathcal{R}}$ for $\mu = \bar{\mu} + \sigma$ and for $\mu = \bar{\mu} - \sigma$ appear as solid and dashed lines.

We now briefly discuss the results and provide some insights gained from the experiments. First, note that the measurements
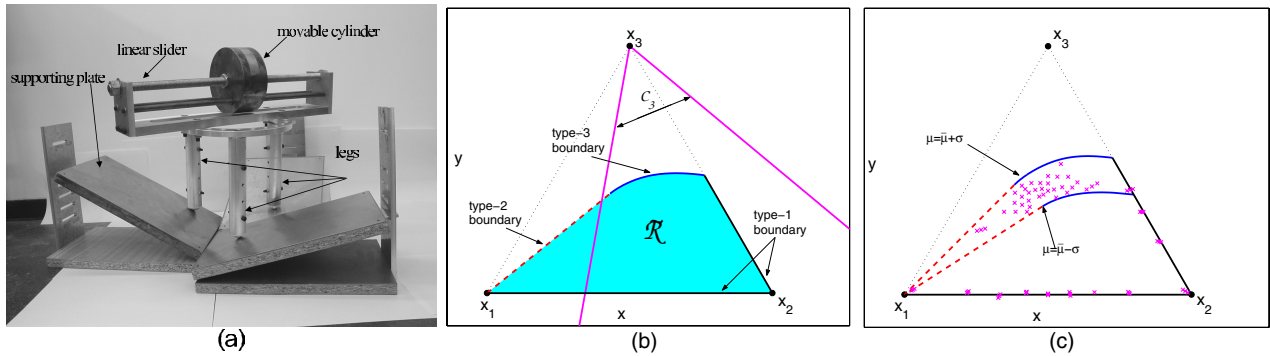
Fig. 3. (a)Experimental setup of a three-legged prototype. (b)Theoretical computation of $\widetilde{\mathcal{R}}$ (shaded region) for $\mu = \bar{\mu}$. (c)Experimental measurements of critical center-of-mass positions ('×') compared with the theoretical boundaries of $\widetilde{\mathcal{R}}$ for $\mu = \bar{\mu} \pm \sigma$ (solid and dashed lines).

associated with the type-1 boundary of $\widetilde{\mathcal{R}}$ have a very small variance and match closely with the theoretical boundary lines. However, the measurements associated with the type-2 and type-3 boundaries of $\widetilde{\mathcal{R}}$ have a much larger variance. Yet all of these points fall within the region computed theoretically for the range $\bar{\mu} \pm \sigma$. Thus the theoretical model of point contact with friction is validated. The reason for the difference in the variances is that type-1 boundaries depend only on geometry of the contacts arrangement. On the other hand, type-2 and type-3 boundaries are highly dependant on the coefficient of friction μ, whose value is determined experimentally, and is subject to large deviations. A possible explanation for the large deviations obtained in measuring μ is the fact that spherical footpads generate point contact with the supports, which is highly sensitive to surface irregularities. A possible solution to this problem can be "flattening" of the footpads to distribute the contact over patches of small area. However, in this case the hard-finger contact model should be replaced by a soft-finger contact model, which includes torques about the contact normals.

VI. CONCLUSION

We have formulated the center-of-mass feasible equilibrium region for three frictional contacts as an intersection of a convex cone and a hyperplane in the six-dimensional wrench space. Using this formulation, we have derived a classification and closed-form expressions of the candidate boundary curves of the feasible equilibrium region. We provided a geometric characterization of the boundary curves, as well as physical interpretation of their corresponding imminent motions. The theoretical computation was illustrated with graphical examples, and validated by experimental results .

Consider now some possible generalizations of this work. First consider a stance with a general number of contacts. In such stances, the support polygon $\widetilde{\Pi}$ is the convex hull of the projected contacts $\tilde{x}_1 \dots \tilde{x}_k$. One first needs to extend the notion of tame stances to multiple contacts. A k-contact stance is *tame* if for any edge $\tilde{x}_i - \tilde{x}_j$ of the support polygon $\widetilde{\Pi}$, all possible torques generated by the contact forces about the line $x_i - x_j$ have the same sign. Using this definition, Theorem 1 generalizes. Namely, it can be shown that for a k-contact tame stance, $\mathcal{R}$ is bounded, and satisfies $\mathcal{R} \subseteq \Pi$. Furthermore,

it can be shown that all boundaries of $\mathcal{R}$ are associated with no more than *three* nonzero critical contact forces. Hence for a k-contact tame stances, the feasible region $\mathcal{R}$ is the *convex hull* of all the feasible equilibrium regions associated with all possible triplets of contacts. $\{x_i, x_j, x_k\}$.

Second, the feasible equilibrium region was computed while considering a single gravitational load. However, in practice one must consider stances which are *robust* with respect to a neighborhood of disturbance wrenches surrounding the nominal gravitational wrench [10]. The characterization of *robust* equilibrium stances in three-dimensional environments is currently under investigation.

REFERENCES

[1] A. Bicchi. On the closure properties of robotic grasping. *The Int. J. of Robotics Research*, 14(4):319–334, 1995.

[2] T. Bretl and S. Lall. A fast and adaptive test of static equilibrium for legged robots. In *IEEE Int. Conf. on Robotics and Automation*, pages 1109 – 1116, 2006.

[3] Li Han, J.C. Trinkle, and Z.X. Li. Grasp analysis as linear matrix inequality problems. In *IEEE Trans. on Robotics and Automation*, 16(6):663–674, 2000.

[4] J. R. Kerr and B. Roth. Analysis of multi-fingered hands. *The Int. J. of Robotics Research*, 4(4):3–17, 1986.

[5] J. Kuffner, K. Nishiwaki, S. Kagami, M. Inaba, and H. Inoue. Motion planning for humanoid robots under obstacle and dynamic balance constraints. In *IEEE Int. Conf. on Robotics and Automation*, pages 692–698, 2001.

[6] R. Mason, J. W. Burdick, and E. Rimon. Stable poses of three-dimensional objects. In *IEEE Int. Conf. on Robotics and Automation*, pages 391–398, 1997.

[7] R.B. McGhee and A.A. Frank. On the stability properties of quadruped creeping gaits. *Mathematical Biosciences*, 3(3–4):331–351, 1968.

[8] Y. Or and E. Rimon. Computing 3-legged equilibrium stances in three-dimensional gravitational environments. In *IEEE Int. Conf. on Robotics and Automation*, pages 1984 – 1989, 2006.

[9] Y. Or and E. Rimon. New results on computing frictional equilibrium stances in three-dimensional gravitational environments. Tech. report, Dept. of ME, Technion, *http://robots.technion.ac.il/publications*, 2006.

[10] Y. Or and E. Rimon. Computation and graphical characterization of robust multiple- contact postures in two-dimensional gravitational environments. *The Int. J. of Robotics Research*, 25(11):1071–1086, 2006.

[11] J. Ponce, S. Sullivan, A. Sudsang, J.-D. Boissonnat, and J.-P. Merlet. On computing four-finger equilibrium and force-closure grasps of poly-hedral objects. *The Int. J. of Robotics Research*, 16(1):11–35, 1997.

[12] T. Sugihara and Y. Nakamura. Whole-body cooperative COG control through ZMP manipulation for humanoid robots. In *2nd Int. Symp. on Adaptive Motion of Animals and Machines (AMAM2003)*, 2003.

[13] M. Vukobratovic, A.A. Frank, and D. Juricic. On the stability of biped locomotion. In *IEEE Trans. Biomed. Eng.*, 17(1):25–36, 1970.